

## **A Study of the Gurson Damage Model and Numerical Simulation of Ductile Failure in LS-DYNA**

Thomas M. Fesich, Pradeep Mohan, Dhafer Marzougui, Cing-Dao (Steve) Kan  
FHWA/NHTSA National Crash Analysis Center  
The George Washington University, United States

### **Summary:**

Standard material models like linear elastic or elastic plastic formulations are not able to precisely reproduce component behavior when failure occurs. Micromechanical damage models enable a more accurate prediction of material behavior, but still require expert knowledge.

In the presented study, the capability of the simple piecewise linear plasticity and the Gurson-Tvergaard-Needleman material model to accurately reproduce and predict physical failure behavior is examined. The main focus is to investigate the capabilities to reproduce stress state and crack growth in a physically meaningful way. Mesh size and material formulation effects are studied on single edge bending and notched tensile specimens.

The results obtained from the different simulations with the GTN model and the piecewise linear plasticity model are compared for conventional finite element simulations and the element-free Galerkin method. Simulations of asymmetric crack growth show that especially the element-free Galerkin method in conjunction with the GTN model provides a powerful tool to simulate failure. With these insights, the accuracy of crash and other failure-related simulations can be improved.

### **Keywords:**

Gurson, element- free Galerkin, mesh-free, crack propagation

## 1. Introduction

Increasing requirements on crash safety of automotive components, but also increasing demand for safe yet light-weight and life cycle cost efficient structures in power plant engineering impose a major challenge on structural engineers: The accurate prediction and numerical simulation of fracture and material failure. While the basic fracture theory is well advanced, numerical simulation of damage still requires expert knowledge and no simple yet general simulation technique is available. The basic challenge in numerical simulation of failure is to combine the right material model that can account for the damage in a physically meaningful way with a suitable discretization and a domain formulation that accurately reproduces the crack propagation and crack growth behavior.

## 2. The Gurson-Tvergaard-Needleman (GTN) Material Model

In 1977, Gurson (1) proposed a damage mechanics material model based on the observation that available plasticity models such as the von Mises model were predicting incompressibility, although ductile fracture could involve significant porosity. Tvergaard (2) as well as Tvergaard and Needleman (3) later modified the basic model. The void volume fraction  $f$  is replaced by the modified damage parameter  $f^*$  in the Gurson-Tvergaard-Needleman (GTN) model to reflect the accelerated void coalescence process after a critical void volume fraction  $f_c$  is reached. Three phenomenological fitting parameters  $q_1$ ,  $q_2$ , and  $q_3$  allow a better fit of numerical results to experiments (4). Today, the Gurson damage model in this modification is the model of choice for crash simulations. The basic yield function of the GTN model is given as:

$$\Phi = \left( \frac{\Sigma_{eq}}{\sigma_0} \right)^2 + 2q_1 f^* \cosh \left( \frac{3}{2} q_2 \left( \frac{\Sigma_h}{\sigma_0} \right) \right) - (1 + q_3 f^{*2}) = 0 \quad (2.1)$$

Here,  $\Sigma_{eq}$  and  $\Sigma_h$  denote the macroscopic equivalent stress and the hydrostatic macroscopic stress, respectively.  $\sigma_0$  is the equivalent tensile yield stress.

For the temperature and strain rate independent GTN-model, a total of nine parameters have to be defined:

The three fitting parameters  $q_1$ ,  $q_2$ , and  $q_3$  are known as “model parameters”, as they influence the form of the yield surface. The three parameters initial void volume fraction  $f_0$ , critical void volume fraction  $f_c$  and fracture void volume fraction  $f_f$  are related to the model of an incompressible matrix with a void. The parameters  $\varepsilon_n$ ,  $s_n$ ,  $f_n$  define the strain controlled void nucleation under load. A modified version of the GTN model that accounts for strain and temperature rate dependent material behavior is not discussed here.

## 3. The Element-Free Galerkin (EFG) Method

The element-free Galerkin method is a new method developed in the 1990s. It is especially useful when simulating crack growth problems, as it does not

require any element connectivity data. Also, distorted nodal arrangements do not lead to poorer accuracy. Cracks in a body are simply modeled by free surfaces, and crack extension is modeled by extending these surfaces. With the EFG formulation, the grid of elements is replaced by a mesh of nodes and a boundary description. Contrary to finite element methods, only the external and internal boundary conditions of the body are defined, but the interior of the domain is filled with unconnected nodes and non-located integration points. The displacement interpolant is then constructed by applying the moving-least-square (MLS) approximation to the nodes that lie close to the given integration point within the surrounding domain.

The mathematical description of the MLS technique can be found e.g. in the works of Belytschko (5) or Hallquist (6). For a trial function  $u(\mathbf{x})$  that is defined in a domain  $\Omega$  which includes the arbitrary spatial point  $\mathbf{x} \in \Omega$ , the small sub-domain (also called support) surrounding  $\mathbf{x}$  is given by  $\Omega_{\mathbf{x}}$  with  $\Omega \supset \Omega_{\mathbf{x}}$ . The function  $u(\mathbf{x})$  can then be expressed as a discrete MLS approximation as

$$u^h(\mathbf{x}) = \{1 \ x \ y \ x^2 \ \dots\} \begin{Bmatrix} a_1(\mathbf{x}) \\ a_2(\mathbf{x}) \\ \vdots \end{Bmatrix} = p_i(\mathbf{x}) b a_i(\mathbf{x}) \quad (3.1)$$

Note that the nomenclature used here follows the literature, but differs from the notation used in LS-DYNA. The basis function monomial  $p_i(\mathbf{x})$  is given as  $H_i(\mathbf{x})$  in LS-DYNA (6), and the coefficients  $a_i(\mathbf{x})$  are given as  $b_i(\mathbf{x})$  with the summation index  $i = 1..n$ .  $n$  denotes the order of completeness of the approximation.

The coefficients  $a_i(\mathbf{x})$  at any point  $\mathbf{x}$  depend on the sampling points  $\mathbf{x}_I$  by a weighting function  $w_a(\mathbf{x} - \mathbf{x}_I)$  defined in the sub-domain  $\Omega_{\mathbf{x}_I}$  (e.g., a disc or a sphere for three-dimensional analysis.)

The discretization process for the EFG is similar to the FEM process, with the only major difference that the trial functions do not satisfy the essential boundary conditions. More details can be found in the referenced literature.

#### 4. Notched Tensile Failure Simulation Results

The capabilities of the GTN model are investigated using micro notched tensile specimen and single edge bending test specimen. The micro notched tensile specimen geometry can be seen in Figure 4-1.

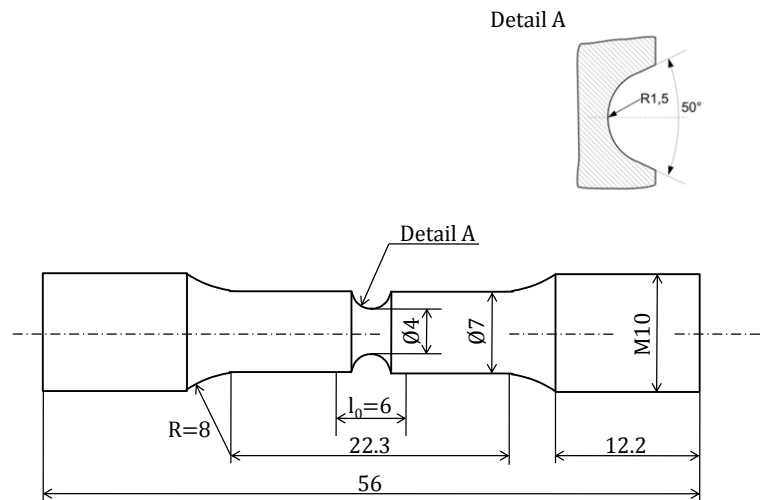


Figure 4-1 : Notched Tensile Specimen FEM Model.

A simulation using the standard elastic-plastic material definition \*MAT\_024 is used to determine the capabilities to simulate tensile tests with simple material models. The mesh is divided into parts so that the layers of elements closest to the smallest cross-section of the specimen (i.e., where crack initiation is expected) can be defined as constant stress solid elements (ELFORM 1) or as fully integrated S/R elements (ELFORM 2), while the rest of the specimen is modeled with the computationally more efficient constant stress solid elements.

The GTN model has been tested with an available parameter set and three different mesh sizes of 0.1 mm, 0.2 mm and 0.4 mm characteristic length. The initial load- displacement behavior of all three meshes is very similar. However, they do show different elongations at rupture. The coarser meshes yield higher elongations at rupture. All three simulations are able to predict the maximum load while predicting different failure strain.

To determine the quality of a numerical simulation of fracture, it is not sufficient to look only at the stress-strain curve, but also to the physical behavior of the model. It is possible to mathematically adjust parameters so that the fracture strain or the maximum stress of the simulation fit the test results. However, also the stress state should be reproduced correctly to obtain a good numerical model.

The multi-axiality can be characterized via the multi-axiality parameter  $q$  (7). This parameter is defined as the quotient of von Mises and hydrostatic stress:

$$q = \frac{\sigma_{vM}}{\sqrt{3}\sigma_h} \quad (4.1)$$

where small values of  $q$  define high triaxiality of the stress state.

An analysis of the multi-axiality parameter is performed for the notched cross-section, where failure is expected, see Figure 4-2.

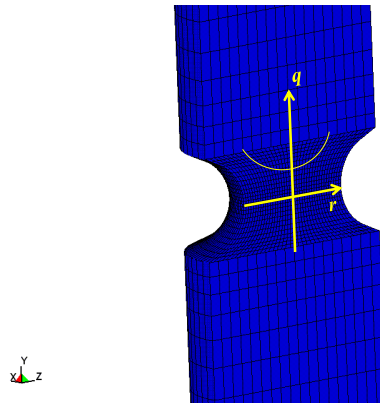


Figure 4-2 : Cross-Section used for Stress Triaxiality Measurements.

It can be seen from Figure 4-3, Figure 4-4 and Figure 4-5, that both material models predict a triaxial stress state throughout the simulation time. However, the difference of triaxiality between the surface and the interior of the specimen differs. The constant stress elements with the piecewise linear plasticity material model show a smaller difference in multi-axiality over the radius of the specimen. This change of stress state is bigger in the simulation that uses fully integrated elements. Still, the curve is flattened in the middle of the specimen, which indicates a constant level of multi-axiality. In contrast, there is a multi-axiality gradient for the GTN material model simulation in the entire specimen. Also, the total values of  $q$  are slightly lower for the Gurson material model which indicates higher multi-axiality.

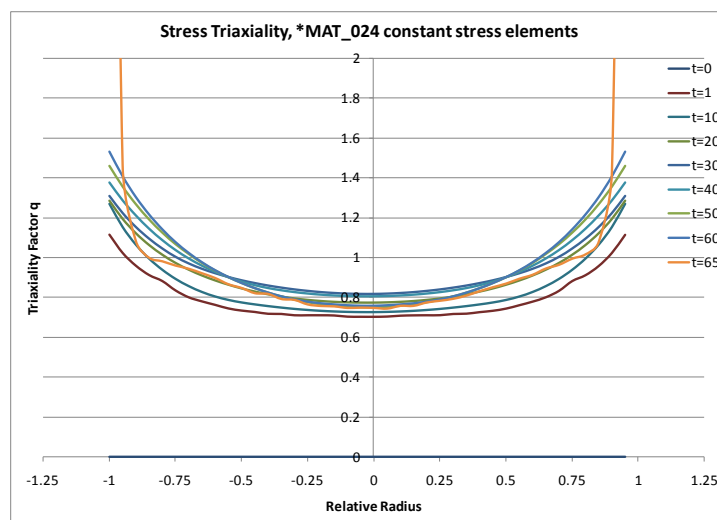


Figure 4-3 : Stress Triaxiality Factor  $q$  for \*MAT\_024 constant stress elements.

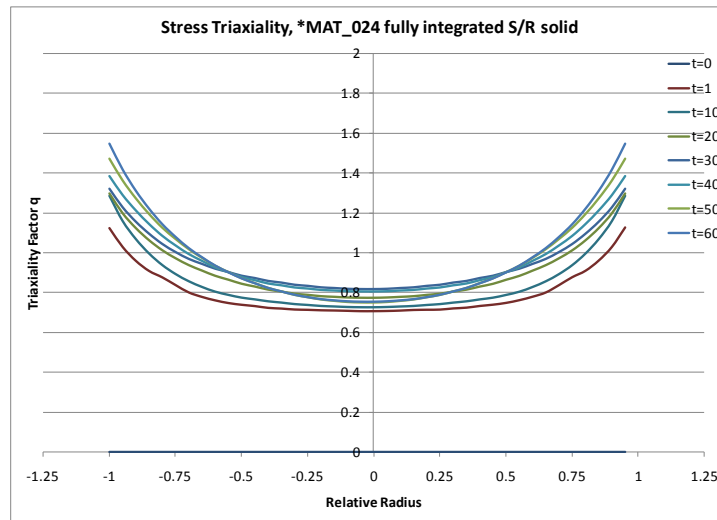


Figure 4-4 : Stress Triaxiality Factor  $q$  for \*MAT\_024 fully integrated S/R elements.

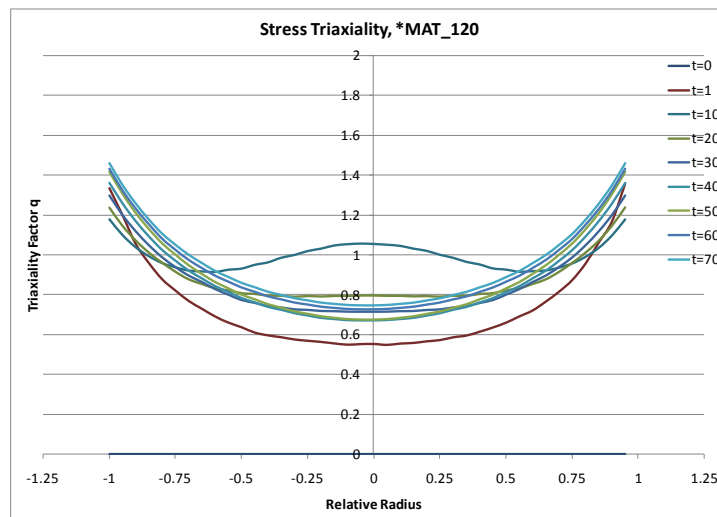


Figure 4-5 : Stress Triaxiality Factor  $q$  for \*MAT\_120.

The distribution of the principal stress and the von Mises stress as well as the development of rupture are compared graphically for the simple piecewise linear plasticity material \*MAT\_024 and the Gurson model \*MAT\_120 in Figure 4-6 to Figure 4-8.

Figure 4-6 and Figure 4-7 show the development of the tensile stress in the notched area of the specimen for the piecewise linear plasticity material model with constant stress and fully integrated S/R elements, respectively. It can be seen that the stress is distributed evenly until fracture initiation occurs on the surface of the specimen. In contrast, for the Gurson model in Figure 4-8, fracture initiates in the middle of the smallest cross-section, which is in accordance to the real behavior. A comparison of the first principal stress distribution and the von Mises stress distribution shows that the von Mises stress in the necking area is decreasing towards the center of the cross-section. This confirms that the stress triaxiality is higher in the center of the cross-section and thus the GTN model predicts the real behavior. Still, a cup-cone fracture form is not simulated even with the GTN material model.

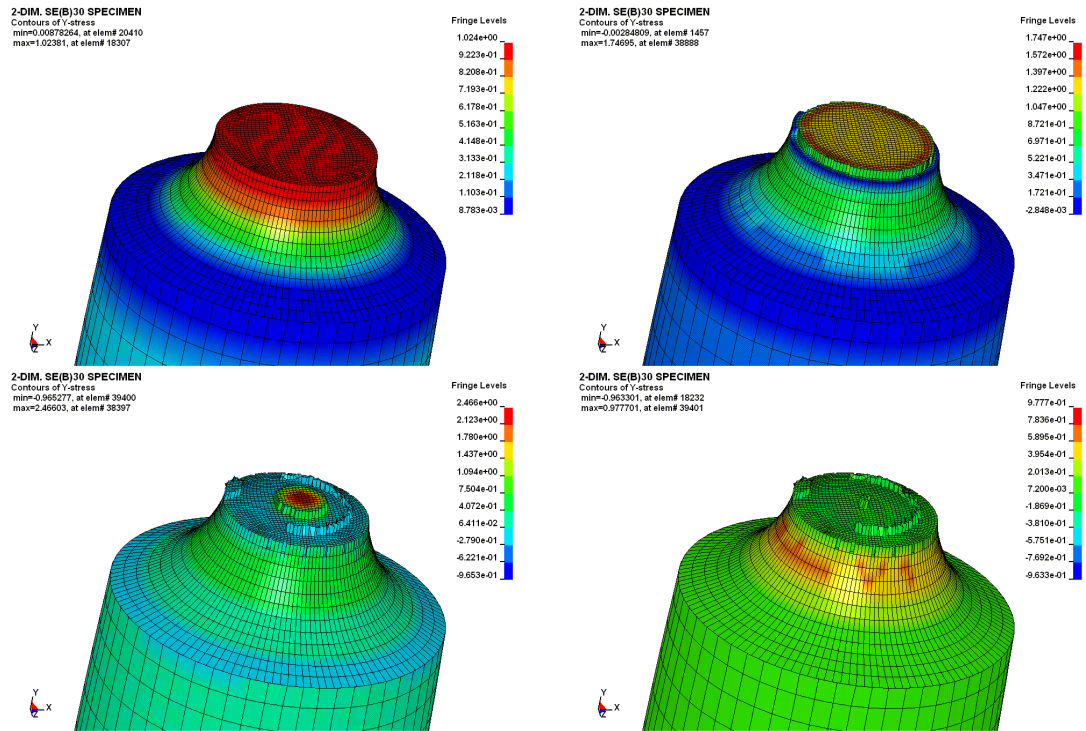


Figure 4-6 : Tensile Stress Development \*MAT\_024 (constant stress elements).

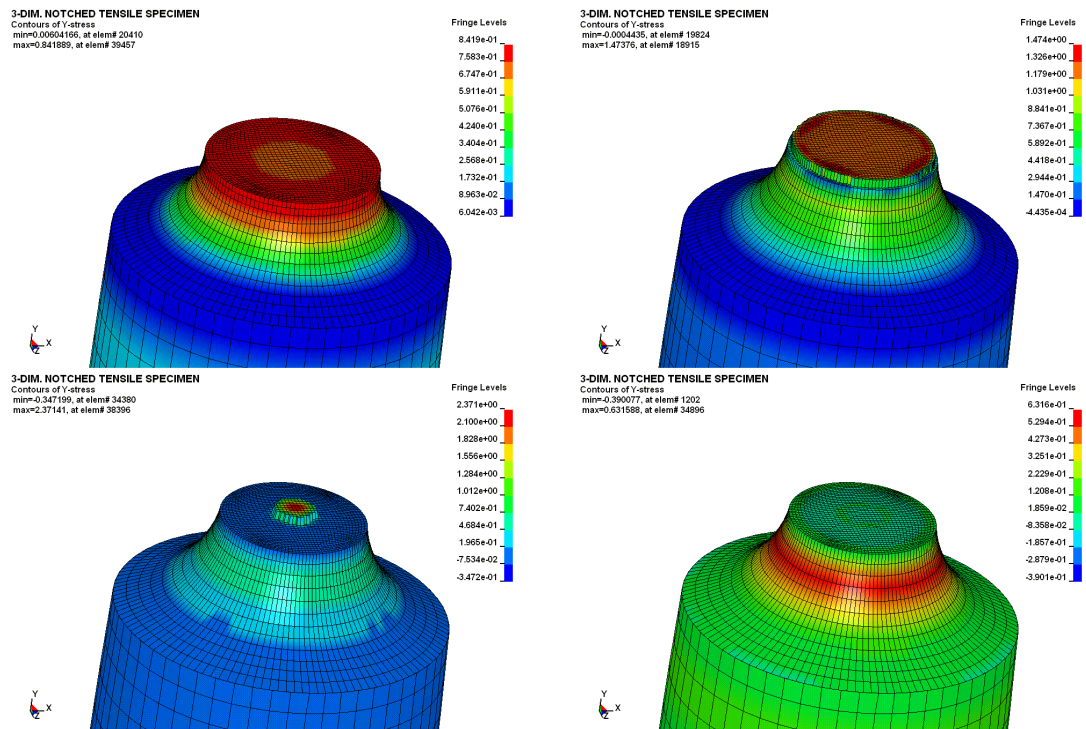


Figure 4-7 : Tensile Stress Development \*MAT\_024 (fully integrated S/R elements).

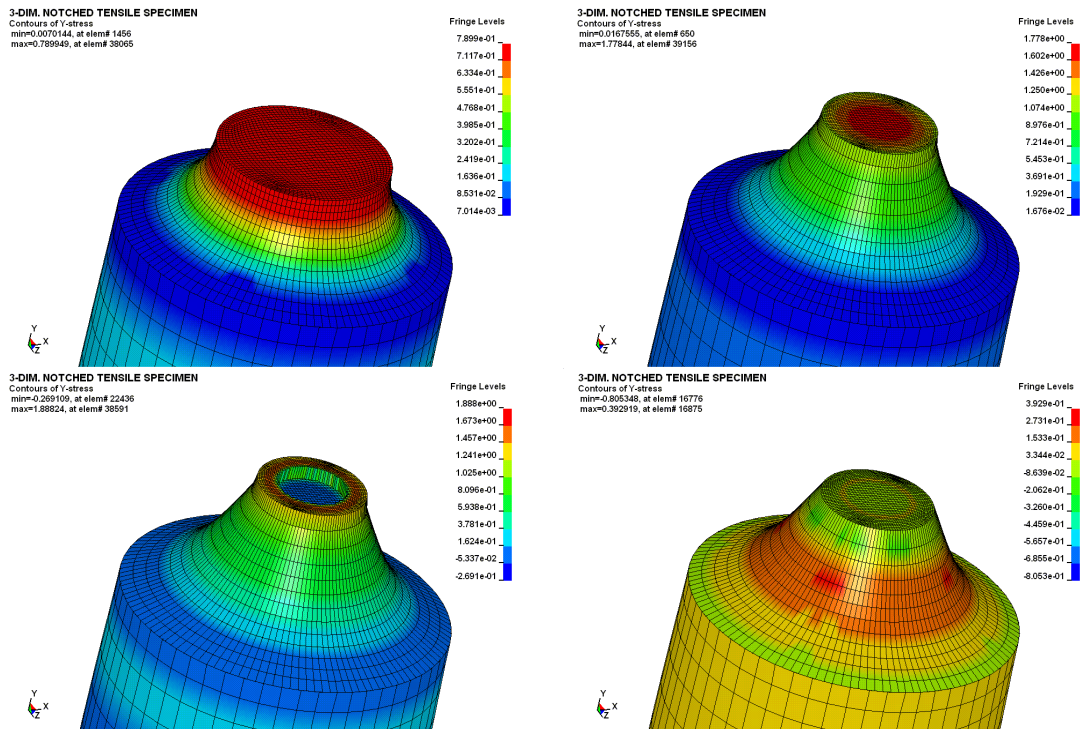


Figure 4-8 : Tensile Stress Development \*MAT\_120 (fully integrated S/R elements).

### 5. Single Edge Bending Simulation Results

In finite element crack growth simulations, mesh geometry and size are crucial factors. Therefore, five different two-dimensional meshes and one three-dimensional mesh are developed and compared. The basic specimen geometry is specified in ASME E 1820 (8) and can be seen in Figure 5-1. The crack is either modeled explicitly as an external boundary of the specimen with a width of one element row, or implicitly by detaching two rows of elements. Three 2D meshes are used to investigate different crack tip meshes, the fourth mesh is an element size variation of mesh three. In addition, one mesh with elements that are rotated 45° relative to the crack propagation direction is tested. None of the two-dimensional meshes is able to accurately predict the force-COD behavior of experimental results. Thus, the three-dimensional model is used to investigate the crack behavior despite the high computational cost.

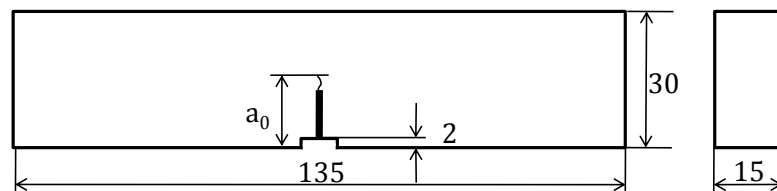


Figure 5-1 : SE(B)30 specimen geometry

In the previous section, the necessity of fracture analysis is described for the notched tensile specimen. It is also important to accurately predict the shape of the crack in the case of SE(B) specimen. The stress in the plane orthogonal to the crack plane and the crack growth are shown in Figure 5-2. It can be seen that the form of the crack front is much more realistic for the Gurson material model.

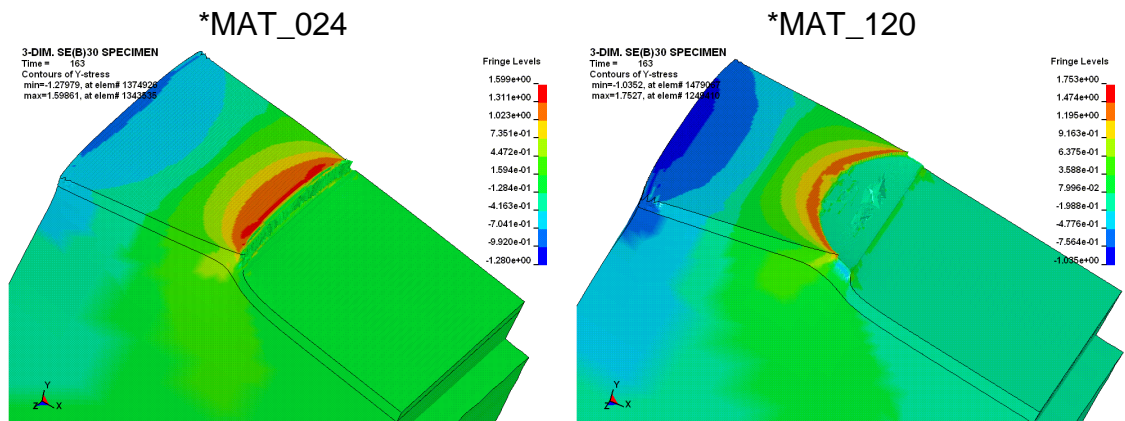


Figure 5-2 : SE(B) Crack Shape and Maximum Y Stress \*MAT\_024 and \*MAT\_120.

### 5.1 Symmetric Crack Growth

In the previous sections, the capabilities of the Gurson material model have been studied using conventional finite element calculations. However, these finite element approaches are limited when large deformations and fracture occurs.

Thus, the SE(B) crack growth has also been analyzed using the element-free Galerkin method. As EFG methods increase the calculation time, only the crack tip region has been modeled as an element-free area. The rest of the specimen uses conventional finite elements.

The crack growth of the conventional finite element simulation and the element-free Galerkin method can be seen in Figure 5-3. Both simulations yield comparable crack growth patterns, but different crack lengths. For the applied COD of approximately 6.5 mm in both cases, the force for the EFG simulation is slightly lower, and the crack growth of the EFG simulation (2.9 mm) is higher than for the FEM simulation (2.4 mm). The overall EFG reaction is thus slightly softer than the traditional FEM simulation. In the pictures, the upper part of the specimen is not shown to visualize the crack.

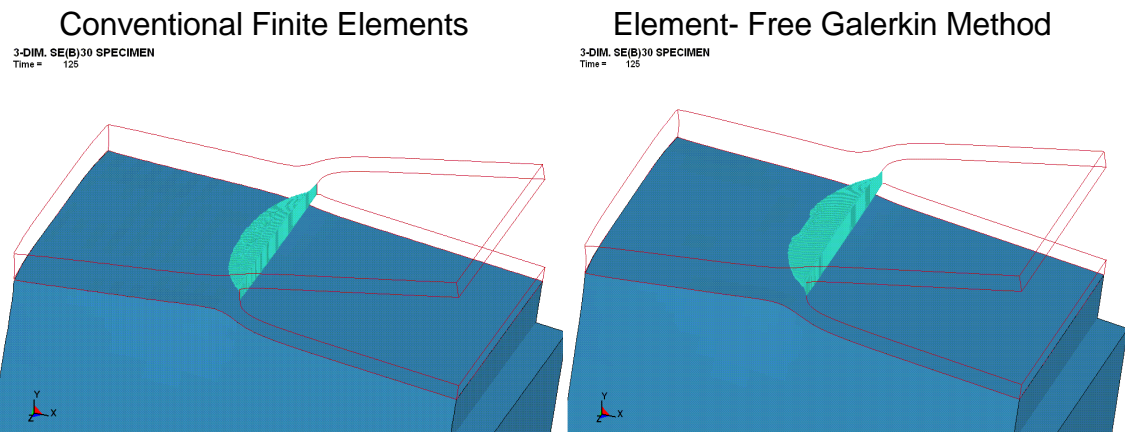


Figure 5-3 : Crack Growth Simulation, Symmetric Three-Point Bending Simulation, COD = 6.5 mm.

## 5.2 Asymmetric Crack Growth

It has been shown in the previous section that the element-free Galerkin method and the traditional finite element approach both yield similar results for the symmetric simulation, as was expected. However, previous studies showed that the finite element method is not suitable to predict crack growth under asymmetric conditions. For these conditions, crack growth is influenced by the principal element direction rather than the actual load conditions. As there is no principal direction in the element-free Galerkin method, the EFG approach should yield considerably better results under asymmetric loading conditions.

To test this, three three-dimensional SE(B) simulations are compared: two simulations use the conventional finite element formulation with constant stress and fully integrated elements, the third uses EFG in the crack tip region. Asymmetric conditions are obtained by setting one of the support cylinders 30 mm closer to the symmetric plane of the test setup, see Figure 5-4. The mesh is adapted so that the new contact area of the specimen with the support cylinder is refined.

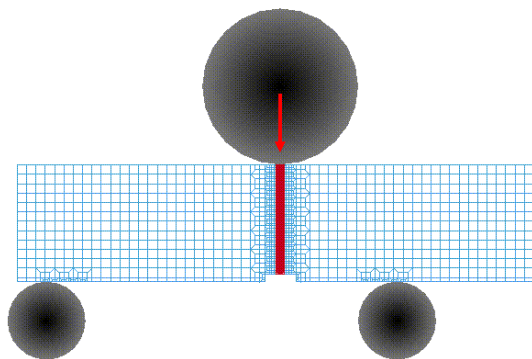


Figure 5-4 : Asymmetric SE(B) Test Setup.

To compare the capabilities of the simulations, the crack growth is analyzed. Figure 5-5 (left) shows the crack growth for the simulation that uses a

conventional finite element mesh with constant stress solid elements. It is obvious that the crack plane is still the x-z plane, although the test setup is now asymmetric. The constant stress solid element formulation is not able to accurately predict the crack growth direction. Also, fully integrated elements cannot predict the asymmetric crack growth, see Figure 5-5 (right).

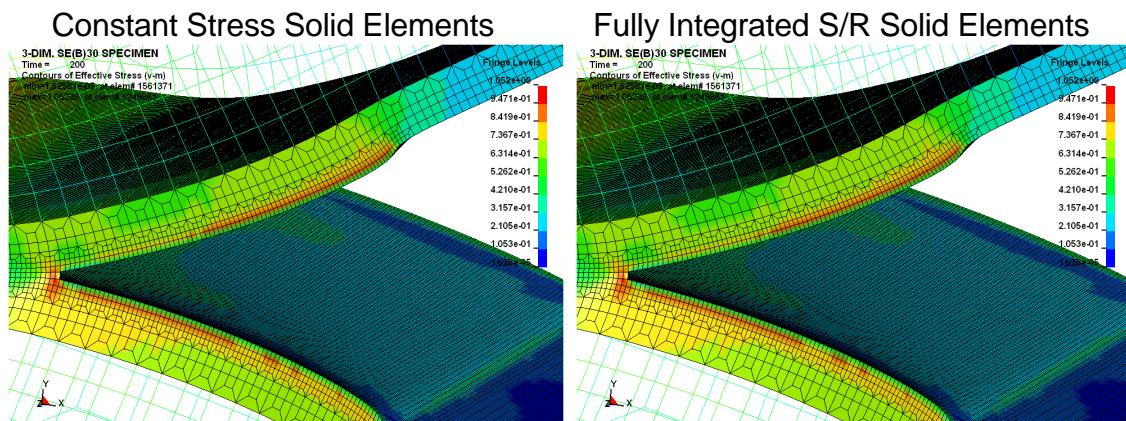


Figure 5-5 : Asymmetric Crack Growth Simulation with Conventional Finite Elements.

By contrast, Figure 5-6 shows the element- free Galerkin simulation for the same simulation setup. It is clearly visible that crack growth deviates from the x-z plane after an initial crack growth in this plane. The EFG approach is able to account for the asymmetric test conditions.

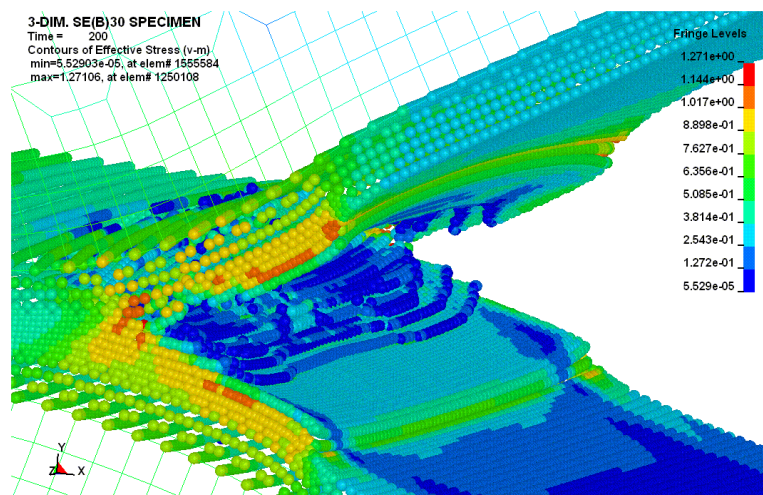


Figure 5-6 : Asymmetric Crack Growth Simulation with the Element- Free Galerkin method.

The advantage of element- free Galerkin methods over the constant stress solids is clearly visible. Only the mesh-free approach is able to predict the asymmetric crack growth and thus eliminates the mesh dependency of the crack propagation.

## 6. Conclusion

The GTN material model enables accurate fracture behavior prediction for notched tensile specimen. The simple elastic-plastic material formulation is not

able to capture the real fracture initiation. For asymmetric conditions or unknown crack propagation direction, conventional finite element approaches are not recommended, as the crack propagation is governed by mesh geometry rather than the load conditions. The element-free Galerkin method is able to predict asymmetric crack growth and thus yields superior results in crack propagation.

## 7. References

1. **Gurson, A.L.** Continuum theory of ductile rupture by void nucleation and growth: Part I-Yield Criteria and flow rules for porous ductile media, Trans. ASME . *J. Eng. Mat. Tech.* 99, 1977, pp. 2-15.
2. **Tvergaard, N.** Influence of voids on shear band instabilities under plane strain conditions. *International Journal of Fracture.* 17, 1981, pp. 389-407.
3. **Needleman, A. and Tvergaard, N.** Analysis of the cup-cone fracture in a round tensile bar. *Acta metall.* 32, 1984, pp. 157-169.
4. **Bernauer, G., et al.** *Hinweise zur Anwendung des GURSON-TVERGAARD-NEEDLEMAN-Modells (Guidelines for the Application of the GURSON-TVERGAARD-NEEDLEMAN-model)*. Geesthacht : GKSS Forschungszentrum, 1999. Technical Note GKSS/WMG/99/10.
5. **Belytschko, T., Lu, Y.Y. and Gu, L.** Element-free Galerkin methods for static and dynamic fracture. *International Journal of Solids and Structures.* 32, 1995, pp. 2547-2570.
6. **Hallquist, J.O.** LS-DYNA® Theory Manual, rev. March 2006. Livermore, CA : Livermore Software Technology Corporation, 2006.
7. **Clausmeyer, H., Kussmaul, K. and Roos, E.** Influence of stress state on the failure behaviour of. *Applied Mechanics Rev.* 44 (2), 1991, pp. 77-92.
8. ASTM E 1820 Standard Test Methods for Measurement of Fracture Toughness. 2008.
9. **Eskandarian, A., Chen, Y.P. and Lee, J.D.** Dynamic meshless method applied to nonlocal crack problems. *Theoretical and Applied Fracture Mechanics.* 38, 2002, pp. 293-300.